

# Propagation of ENSO temperature signals into the middle atmosphere: A comparison of two general circulation models and ERA-40 reanalysis data

R. García-Herrera,<sup>1</sup> N. Calvo,<sup>1</sup> R. R. Garcia,<sup>2</sup> and M. A. Giorgetta<sup>3</sup>

Received 11 April 2005; revised 17 November 2005; accepted 9 December 2005; published 16 March 2006.

[1] The vertical propagation of the El Niño–Southern Oscillation (ENSO) temperature signal has been analyzed in two general circulation models, the Whole Atmosphere Community Climate Model and the Middle Atmosphere European Center–Hamburg Model, and in the ERA-40 reanalysis data set. Monthly mean data have been used, and composite differences (El Niño–La Niña) have been computed. Our results show that the ENSO signal propagates into the middle atmosphere by means of planetary Rossby waves. Significant wave-like anomalies are observed up to around 40 km. This propagation is strongly influenced by the zonal mean zonal winds, being most effective in midlatitudes of the Northern Hemisphere because ENSO events tend to peak in northern winter, when stratospheric winds are westerly in the Northern Hemisphere, and allow vertical propagation of Rossby waves. In addition, zonal mean temperature anomalies are observed in the middle atmosphere in the tropics and at polar latitudes of the Northern Hemisphere. These anomalies are the result of changes in the residual mean meridional circulation: Our analysis reveals that during an El Niño event, vertical wave propagation and divergence of Eliassen–Palm flux are enhanced, forcing a stronger residual circulation in the stratosphere, which cools the tropics and warms the higher latitudes. This pattern is highly significant in the models during certain months but much less in the ERA-40 data, where other sources of variability (in particular the quasi-biennial oscillation) also influence the residual circulation.

**Citation:** García-Herrera, R., N. Calvo, R. R. Garcia, and M. A. Giorgetta (2006), Propagation of ENSO temperature signals into the middle atmosphere: A comparison of two general circulation models and ERA-40 reanalysis data, *J. Geophys. Res.*, *111*, D06101, doi:10.1029/2005JD006061.

## 1. Introduction

[2] The effects of El Niño–Southern Oscillation (ENSO) on atmospheric temperatures have been widely investigated in the troposphere where ENSO is known to be one of the main sources of variability. During the last two decades, many authors have focused on analyzing the relationship between ENSO and tropospheric temperatures, both in the tropics [Angell, 1981; Christy and McNider, 1994; Angell, 2000], and at extratropical latitudes [Kiladis and Diaz, 1989; Halpert and Ropelewski, 1992; Díaz *et al.*, 2001]. The influence of ENSO in the stratosphere has not been analyzed so extensively. Several studies have investigated the role of ENSO in the extratropical stratospheric circulation by using observational data [Wallace and Chang, 1982; van Loon and Labitzke, 1987; Hamilton, 1993; Baldwin and

O’Sullivan, 1995]. Other works have focused on the effects of ENSO on temperatures. Thus Reid *et al.* [1989] used several radiosonde stations over the Pacific Ocean to study the ENSO signal in the tropics, and Yulaeva and Wallace [1994] and Calvo *et al.* [2004] used satellite data from the Microwave Sounding Unit (MSU) to analyze the signature at both tropical and extratropical latitudes. Nevertheless, the influence of ENSO in the middle atmosphere has not been thoroughly documented, mainly because of the lack of observations from the stratosphere and mesosphere. This is one of the main reasons why general circulation models (GCMs) have become one of the few tools available to investigate the ENSO phenomenon in the middle atmosphere.

[3] Most GCMs have been developed to study tropospheric climate, even though they have usually included at least the lower stratosphere in order to avoid problems that would result from imposing a rigid lid upper boundary condition at the tropopause. Aside from those tropospheric/lower stratospheric models, a few groups developed troposphere/stratosphere or troposphere/stratosphere/mesosphere GCMs, commonly known as middle atmosphere GCMs, on the basis of either their existing tropospheric GCMs or troposphere/stratosphere GCMs. Two recently developed

<sup>1</sup>Departamento de Física de la Tierra II, Universidad Complutense de Madrid, Madrid, Spain.

<sup>2</sup>National Center for Atmospheric Research, Boulder, Colorado, USA.

<sup>3</sup>Max Planck Institute for Meteorology, Hamburg, Germany.

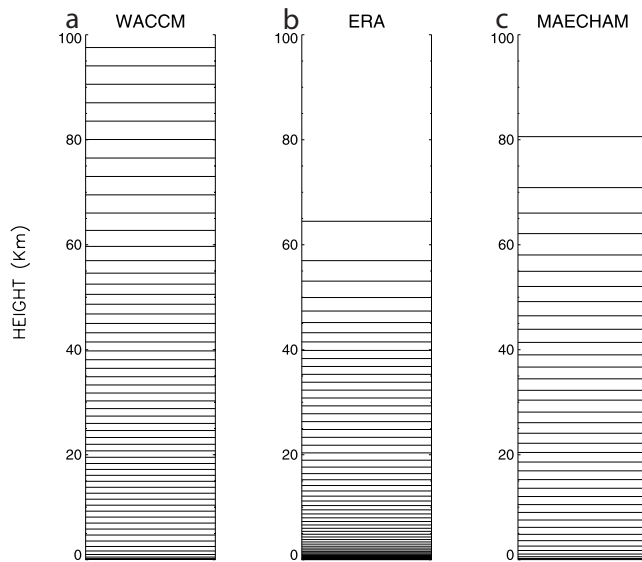


**Figure 1.** Vertical distribution of the model levels for (a) WACCM, (b) ERA-40, and (c) MAECHAM5 data used in this study.

models, the Whole Atmosphere Community Climate Model (WACCM), from the National Center for Atmospheric Research (NCAR), and the Middle Atmosphere European Center–Hamburg Model 5 (MAECHAM5), from the Max Planck Institute for Meteorology, provide a good opportunity to study the propagation of ENSO signals to the middle atmosphere. Both models extend throughout the mesosphere and, in the case of WACCM, into the lower thermosphere. None of the WACCM and MAECHAM5 experiments of this study develops a quasi-biennial oscillation (QBO), which in the present context may be considered an advantage, since it allows the study of ENSO signals without the additional source of variability due to the QBO. Some aspects of the response of these models to SSTs are discussed by *Sassi et al.* [2004] and *Manzini et al.* [2006]. A more in-detail comparison between them following the same methodology and selecting the same extreme ENSO events is carried out in this paper and will provide new insights as will be shown later. In addition to these models, the new ERA-40 reanalysis, with a top boundary in the lower mesosphere, is a third source of data that can be compared to the models. Because the ERA-40 data include variability arising from other sources, such as the QBO and radiative effects of volcanic aerosols, the comparison among ERA-40 and the two models allows investigation of the relationship between ENSO and other sources of variability in the middle atmosphere.

[4] The aim of this paper is to characterize the ENSO signal in atmospheric temperatures, focusing on the middle atmosphere, and to investigate its transmission from the troposphere. To do so, we have used data from the ERA-40 reanalysis, together with output from WACCM and MAECHAM5 simulations covering the period 1979–1999. Section 2 includes a brief description of the most relevant characteristics of the models and the reanalysis data. The main results are described in section 3, while sections 4 and 5 discuss in detail some of the mechanisms involved in the

propagation of the ENSO signal. Conclusions are summarized in section 6.

## 2. GCMs and ERA-40 Data

[5] WACCM version 1b (WACCM1b) has been used in this study. The model is based on the NCAR Community Climate Model version 3 [*Kiehl et al.*, 1998], with suitable extensions for describing physical and radiative processes in the mesosphere and lower thermosphere, as discussed by *Sassi et al.* [2002]. Below we give a brief summary of its salient features.

[6] WACCM1b has 66 vertical levels from the surface to  $5.1 \times 10^{-6}$  hPa or about 140 km. The vertical coordinate is purely isobaric above 100 hPa, but it is a hybrid coordinate below that level. The standard vertical resolution is variable, ranging from 1.1 km in the troposphere (except in the boundary planetary layer where much higher vertical resolution is used) to about 3.5 km in the upper mesosphere. Beyond the mesopause, the vertical resolution is one half the local scale height. Figure 1a shows the vertical structure of the model. The horizontal resolution is T63 with  $128 \times 64$  (longitude by latitude) points in a quasi-linear grid [*Williamson*, 1997]. The dynamical equations are solved using a semi-Lagrangian technique [*Williamson and Olson*, 1994], with a time step of 1800 s.

[7] Some additional physical processes have been added to the CCM3 physics package to simulate the middle and upper atmosphere. Among others, nonlocal thermodynamic equilibrium infrared transfer has been incorporated, the parameterization of gravity wave breaking and diffusion has been extended and molecular diffusion and diffusive separation effects have been taken into account above 90 km. As mentioned earlier, the model does not produce a QBO. Specified sea surface temperatures (SSTs) are introduced in the model as boundary conditions. For this study, we have used monthly mean temperature data from a 50-year simulation, from 1950 to 2000.

[8] ECHAM5 is the most recent version of the Max Planck Institute for Meteorology Atmospheric General Circulation model [*Roeckner et al.*, 2003]. It was initially developed from the European Center for Medium-Range Weather Forecast (ECMWF) model. The configuration that resolves the atmosphere up to 0.01 hPa ( $\sim 80$  km), known as the Middle Atmosphere ECHAM5 (MAECHAM5), has been used in this study [*Manzini et al.*, 2006]. Figure 1c shows the vertical resolution of the 39-layer grid used here. Differences between ECHAM5 and MAECHAM5 include parameterization of momentum flux deposition due to gravity waves and a few modifications in the representation of the horizontal diffusion near the top layer. The main improvements in MAECHAM5 with respect to the previous version [*Roeckner et al.*, 1996; *Manzini et al.*, 1997] comprise the treatment of radiation processes, surface fluxes and cloud physics.

[9] The MAECHAM5 run used for the present study has 39 vertical levels and its vertical resolution in the stratosphere ranges from 1.5 km at the tropical tropopause to 3 km at the stratopause. This resolution does not allow the model to develop a QBO as demonstrated for a higher vertical resolution version of MAECHAM5 [*Giorgetta et al.*, 2002]. The horizontal resolution is T42 with  $128 \times$

**Table 1.** Central Month and Its Corresponding N3.4 Value for the Strongest Warm and Cold ENSO Events Considered in This Study for the Period 1979–1999

| Date                    | N3.4 Value |
|-------------------------|------------|
| <i>Warm ENSO Events</i> |            |
| January 1983            | 2.74       |
| January 1992            | 1.82       |
| December 1994           | 1.32       |
| November 1997           | 2.76       |
| <i>Cold ENSO Events</i> |            |
| December 1984           | −1.21      |
| November 1988           | −1.91      |
| December 1998           | −1.54      |

64 grid points in longitude versus latitude. Sea Surface Temperatures are prescribed in the model as lower-boundary conditions. The experiment used here is forced with observed SSTs from 1978 to 1999. Overall, the WACCM1b and MAECHAM5 experiments analyzed here are very similar, the main difference being the extent of the vertical domain.

[10] Finally, temperature data from the ERA-40 reanalysis have also been used. The ERA-40 reanalysis [Simmons and Gibson, 2000; Uppala *et al.*, 2004; Randel *et al.*, 2004] runs from 1957 to 2002 and is based on the ECMWF three-dimensional variational assimilation system, making com-

prehensive use of satellite and conventional observations. It utilizes multichannel satellite radiances starting with data from the first VTPR sounding instrument in 1972 and continuing up to the present SSM/I, TOVS and ATOVS instruments. The atmospheric model was forced with observed sea surface temperatures. ERA-40 has 60 vertical levels (Figure 1b) with the top at 64 km (0.1 hPa) and T159 spectral resolution. For this study, we used a grid of  $144 \times 73$  (longitude versus latitude) points and monthly mean data. While Randel *et al.* [2004] found cold temperature biases in the upper stratosphere in this data set, this is mitigated somewhat by computing warm minus cold events differences, which should remove to a large extent systematic biases.

[11] To characterize the timing and intensity of ENSO, the Niño 3.4 SST index (hereafter N3.4) has been chosen. The index is computed using SST anomalies for the so-called Niño 3.4 region, which is located between  $5^{\circ}\text{S}$  to  $5^{\circ}\text{N}$  in latitude and  $120^{\circ}\text{W}$  to  $170^{\circ}\text{W}$  in longitude. SST data come from the NCEP Reynolds SST data set, <http://podaac.jpl.nasa.gov/reynolds/>.

### 3. ENSO Signal in the Middle Atmosphere

[12] Composite differences of temperature between the strongest El Niño and La Niña events during the period 1979–1999 have been computed at different latitudes. Monthly temperature data from WACCM, MAECHAM5

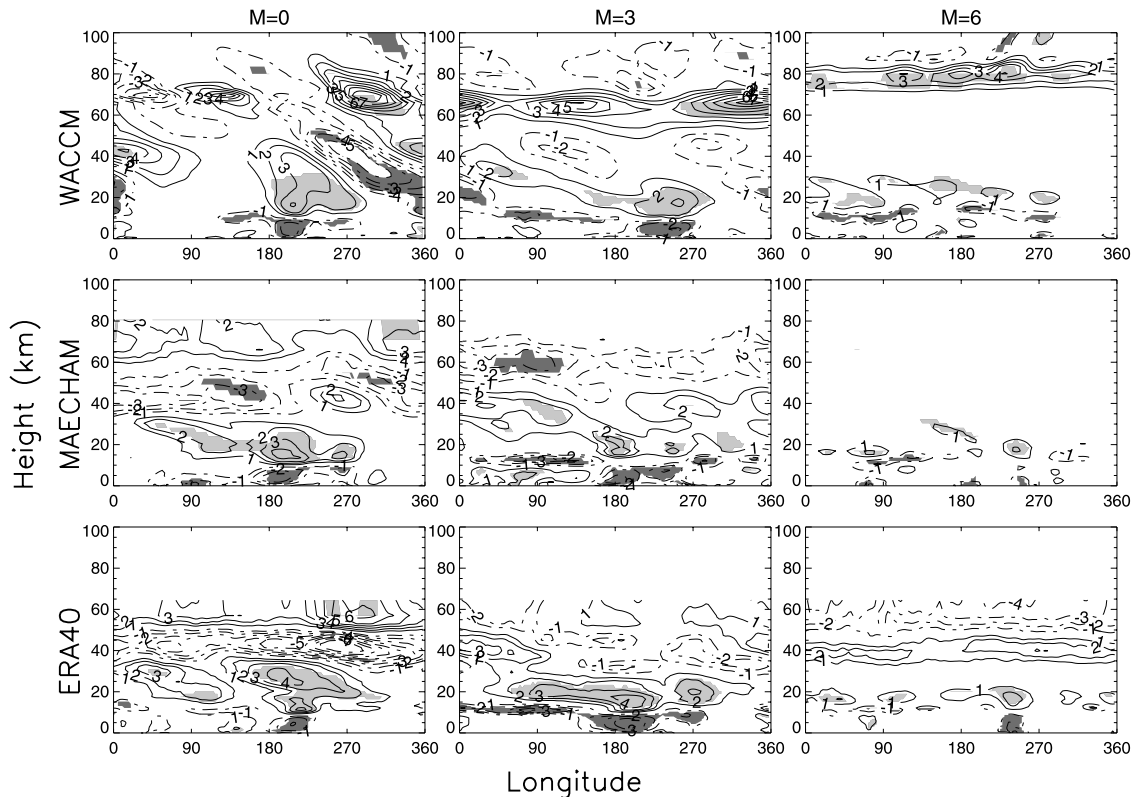


**Figure 2.** Composite differences (warm-cold events) of temperature anomalies from (top) WACCM, (middle) MAECHAM5, and (bottom) ERA-40 data at  $40^{\circ}\text{N}$  in months (left) 0, (middle) 3, and (right) 6. Solid (dashed) lines denote positive (negative) anomalies. Contour interval is  $1^{\circ}\text{C}$ . Zero contour has not been displayed. Shaded regions indicate statistically significant anomalies at the 95% confidence level. Light (dark) gray indicates positive (negative) significant anomalies.

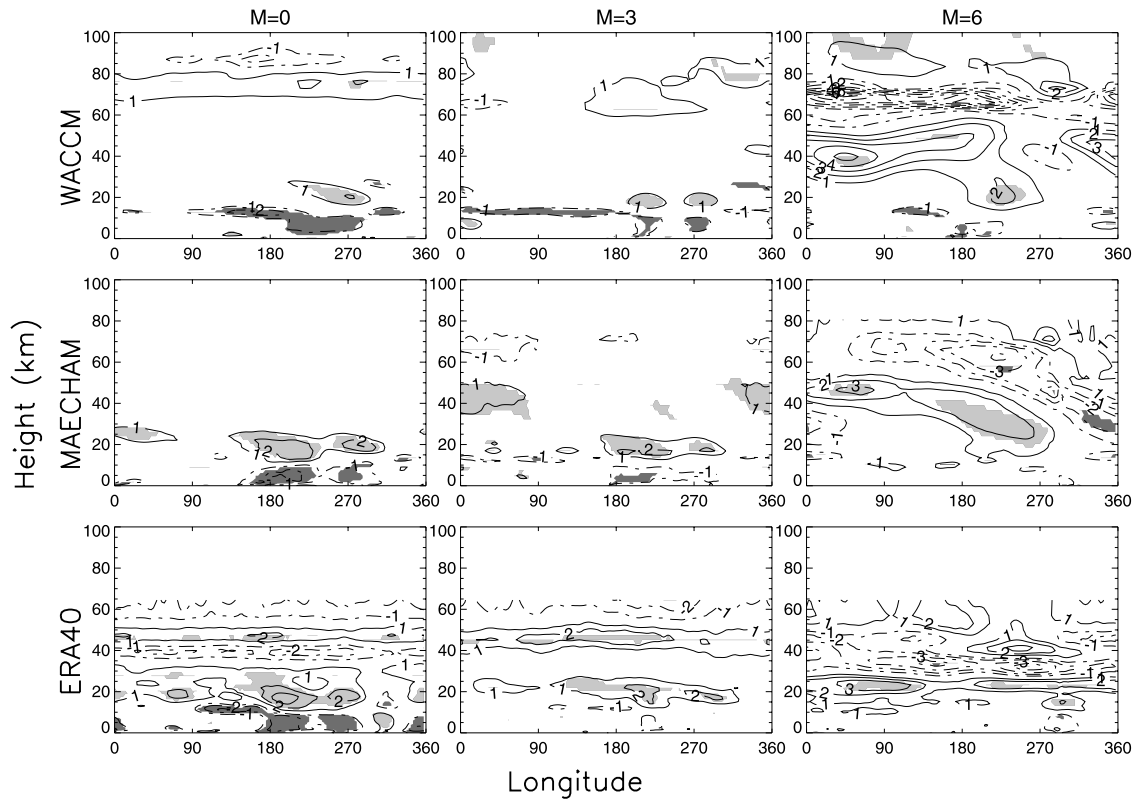


**Figure 3.** As in Figure 2 but at 40°S.

and ERA-40 have been initially treated to eliminate the annual cycle and to remove linear trends. Short-period fluctuations (2–3 months) were smoothed by applying a 1-2-1 filter at every grid point.

[13] The strongest ENSO events have been chosen according to the monthly values of N3.4. The reference date of every warm (cold) event, month 0 in all the composites, has been taken as the date of maximum (minimum) N3.4 whenever this index exceeds 1.2 standard deviations. The events selected are shown in Table 1. All the maxima and minima occur in late fall to early winter. The strong warm event of 1988 has not been considered in this analysis as it peaks in August and this anomalous phasing with respect to the seasonal cycle could confound the interpretation of the ENSO signal, especially outside the tropics.

[14] In the following analysis, composite maps of El Niño–La Niña differences are typically shown every three months, starting at the month of maximum N3.4 (month 0). Thus a composite map for month 3 displays conditions 3 months after the maximum of N3.4. In the composites, the significance of the ENSO anomalies with respect to the internal variability of each data set (model outputs or reanalysis data) has been tested by a Monte Carlo method. First, random groups of 4 and 3 months corresponding to the months of the 4 strongest El Niño and 3 strongest La Niña events used in the composites have been chosen. Then, differences between these groups have been computed 500 times and the distribution plotted. A preliminary analysis showed that 500 realizations were enough to estimate the probability distribution properly. The sample follows a

normal distribution, so that the 5% tails lie at approximately  $\pm 1.96$  standard deviations from the mean. These are the thresholds above or below which the anomalies are considered significant.

[15] Figure 2 depicts the composite differences (El Niño minus La Niña events) for atmospheric temperature anomalies obtained from WACCM, MAECHAM5 and ERA-40, in a longitude-height domain at 40°N. This latitude has been chosen as representative of middle latitudes in the Northern Hemisphere (NH). Shaded regions show the significant anomalies according to the Monte Carlo test.

[16] At 40°N, most of the significant anomalies are located in the troposphere and stratosphere, over the Pacific Ocean. Some of these areas correspond to some of the regions of the Pacific–North America pattern (PNA) [Wallace and Gutzler, 1981; Horel and Wallace, 1981], which is known to be related to ENSO [Horel and Wallace, 1981; Hoskins and Karoly, 1981; Simmons *et al.*, 1983; Ribera and Mann, 2002]. The PNA teleconnection is associated with robust height anomalies over northern Pacific and Northwestern Canada. At middle latitudes in the northern Pacific, the PNA is characterized by a cold troposphere and warm lower stratosphere east of the date-line [Calvo *et al.*, 2004] as it is well seen in Figure 2. In addition, patterns characteristic of ultralong Rossby waves are observed in both the models and the reanalysis. These patterns tilt westward with height, as expected for upward propagating Rossby waves. Significant anomalies are observed up to about 35–40 km and they are especially noticeable in WACCM in month 0. In month 3, WACCM and MAECHAM5 show similar patterns reaching 40 km,



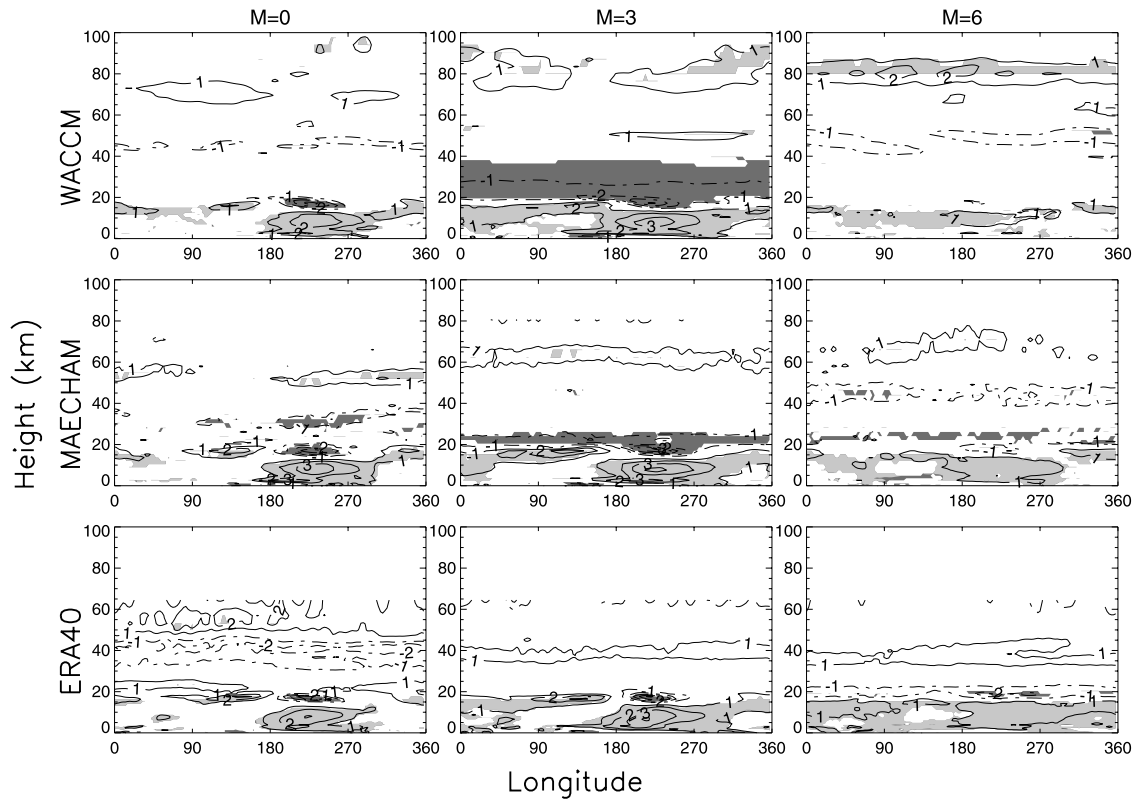


**Figure 4.** As in Figure 2 but at 10°N.

while ERA-40 does not exhibit a significant signal above 30 km. Instead, the anomalies in ERA-40 are confined to the lower stratosphere with little westward tilt, indicating less vertical propagation. Six months after the maximum of N3.4 (month 6), the anomalies have almost disappeared in all the data sets. Maximum values of the anomalies are observed at months 0 and 3 and reach values over 4 K.

[17] In the Southern Hemisphere (SH), the ENSO-related anomalies at middle latitudes also have the shape of wave patterns (Figure 3 shows the composite differences at 40°S), but propagation into the stratosphere seems far less effective, the anomalies are weaker, the significant regions are smaller, and they reach lower heights with the exception of month 6, where MAECHAM5, and to a lesser extent WACCM, shows a significant stratospheric signal. The difference in the efficiency of vertical propagation of the ENSO signal between the SH and the NH could be related to phasing of ENSO events with respect to the seasonal cycle. The events tends to peak in NH winter, when local winds are westerly and allow propagation into the stratosphere. The role of stratospheric winds in controlling the vertical propagation of ENSO signals is discussed in detail in section 4.

[18] At tropical latitudes, the patterns observed are quite different from those in the extratropics. Figure 4 shows the composite differences at 10°N. This latitude is chosen instead of the Equator because wave-like ENSO anomalies over the tropical Pacific Ocean have the form of Rossby gyres, with maxima on either side of the equator, around 10°–15° [cf. Calvo *et al.*, 2004]. The patterns are nevertheless similar when the analysis is carried out at other

tropical latitudes (not shown). WACCM, MAECHAM5 and ERA-40 show almost identical results below 20 km: a center of positive anomalies over the Eastern Pacific and a small center of negative anomalies above it. As noted above, these anomalies have the shape of the forced Rossby gyres, presumably excited by anomalous convection accompanying ENSO events in the tropical Pacific Ocean [García and Salby, 1987; Horinouchi and Yoden, 1996]. This wave-like signal over the Pacific is limited to heights below 15–20 km with maximum values in months 0 and 3. During months 3 and 6, positive anomalies are more zonally uniform spread throughout the tropical troposphere; this agrees well with the behavior documented in several previous studies that used observations in the troposphere. [Angell, 1981; Christy and McNider, 1994; Yulaeva and Wallace, 1994; Calvo *et al.*, 2004]. Above the lowermost stratosphere, MAECHAM5 and WACCM show nearly zonally symmetric negative anomalies in certain months. This is seen in MAECHAM weakly in months 0 and 6 and more strongly in month 3 around 20–25 km. On the other hand, WACCM shows significant anomalies only during month three but in a deeper region from 20 to 35 km. Anomalies in ERA-40 are in the right sense to match the models above 20 km although they are not significant which may be due to the presence of QBO-related variability in ERA-40. The N3.4 composite differences of ERA-40 are not balanced with respect to westerly and easterly QBO phases so that a nonnegligible zonally symmetric QBO related temperature signal must be expected. The presence of such variability will obscure and reduce the statistical significance of ENSO anomalies. Therefore, in the tropical

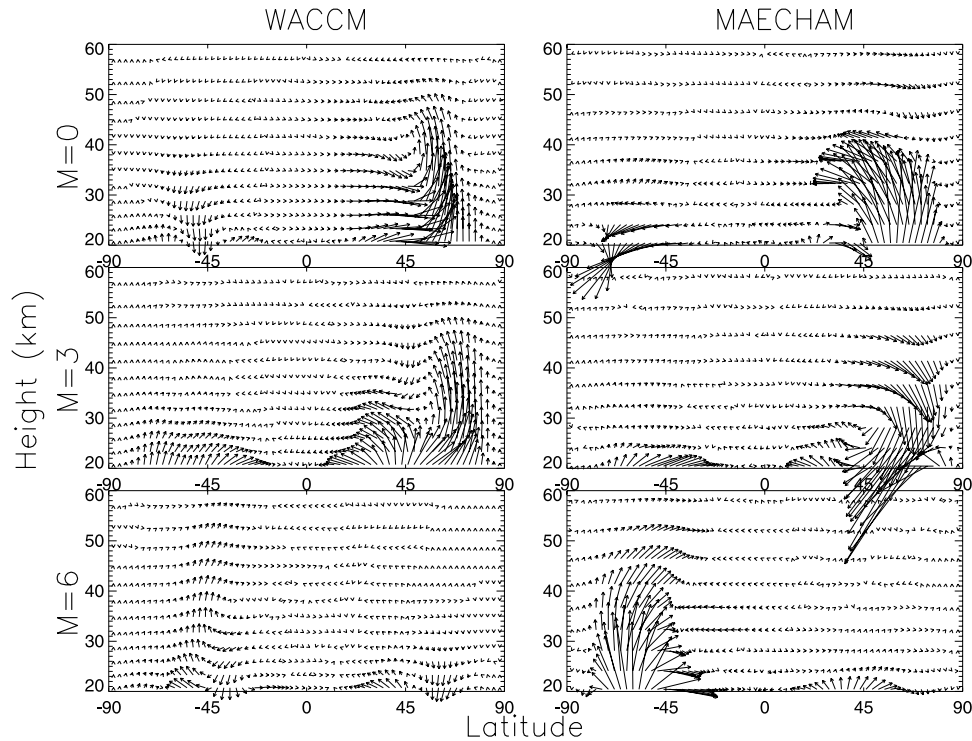


**Figure 5.** Composite differences (warm-cold events) of the Eliassen-Palm flux anomalies from (left) WACCM and (right) MAECHAM5 data, in months (top) 0, (middle) 3, and (bottom) 6. Values drawn are  $F_y \times 10^{-5} \text{ kg s}^{-2}$  and  $F_z \times 5.10^{-4} \text{ kg s}^{-2}$ .

stratosphere, the comparison between the models and ERA-40 results must be interpreted cautiously.

[19] Despite the differences among WACCM, MAECHAM5 and ERA-40, the results are broadly consistent in many respects across the models and the reanalysis. A correlation analysis further corroborates these results. Longitude-height grid point lag correlations were computed between temperature and N3.4 at different latitudes. Autocorrelation effects were taken into account in the assessment of significance [Oort and Yienger, 1996]. These correlation maps (not shown) exhibit patterns coherent with those from the composite analysis both in the tropics and extratropics. The same vertical structure of the ENSO signature is observed, which increases the confidence in the results of the composite analysis.

[20] In short, our analysis suggests that Rossby waves propagate ENSO anomalies vertically into the middle atmosphere at middle latitudes, particularly in the NH, in good agreement with results from Sassi *et al.* [2004] and Manzini *et al.* [2006]. However, the wave ENSO signal is not observed beyond the lower stratosphere in tropical latitudes. Rossby wave propagation may be further visualized by means of Eliassen-Palm (EP) flux cross sections. Figure 5 shows composite differences (El Niño–La Niña events) of anomalies of EP flux for WACCM and MAECHAM5 during months 0, 3 and 6. The EP flux vectors can be considered as a measure of wave propagation from one height and latitude to another [Edmon *et al.*, 1980]. Thus, at middle latitudes in month 0, the figures show clear evidence of enhanced upward propagation in the NH and reduced propagation in the SH (referred to climatology), the former being much more intense. This is

consistent with the patterns observed in the temperature composites (Figures 2 and 3), which showed significant anomalies at higher altitudes in the NH than in the SH. During a warm ENSO (El Niño) event, vertical wave propagation is enhanced in the Northern Hemisphere whereas it is reduced during the opposite phase of ENSO (not shown). WACCM shows more poleward propagation in the NH from 20 to 30 km in the region between 25° and 50°N and a well defined propagation channel at 60°N up to heights around 55 km, where the waves start to bend toward the Equator. MAECHAM5 shows larger EP fluxes anomalies in the lower stratosphere but the waves are refracted toward the Equator at lower heights than in WACCM, around 35 km. This is consistent with the differences between the two models observed in the NH in Figure 2, where WACCM showed greater westward tilt, indicative of more effective vertical propagation. In month 3, the region from 25°N to 45°N shows positive vertical anomalies of EP flux in both WACCM and MAECHAM5, whereas poleward of 45°N, wave propagation is enhanced in WACCM but reduced in MAECHAM5 (with respect to climatology). Finally, 6 months after the N3.4 maximum, the pattern is almost the reverse of that in month 0, and wave propagation is enhanced mainly in the SH, being more intense in MAECHAM5, which is also consistent with our results for temperatures in Figure 3. Figure 3 showed significant anomalies propagating upward in MAECHAM5 but not in WACCM in that month.

[21] Considering all these results, it is important to note how the patterns of ENSO-related temperature anomalies depend on latitude. To provide comprehensive view, we have displayed the composite differences for month 0 at

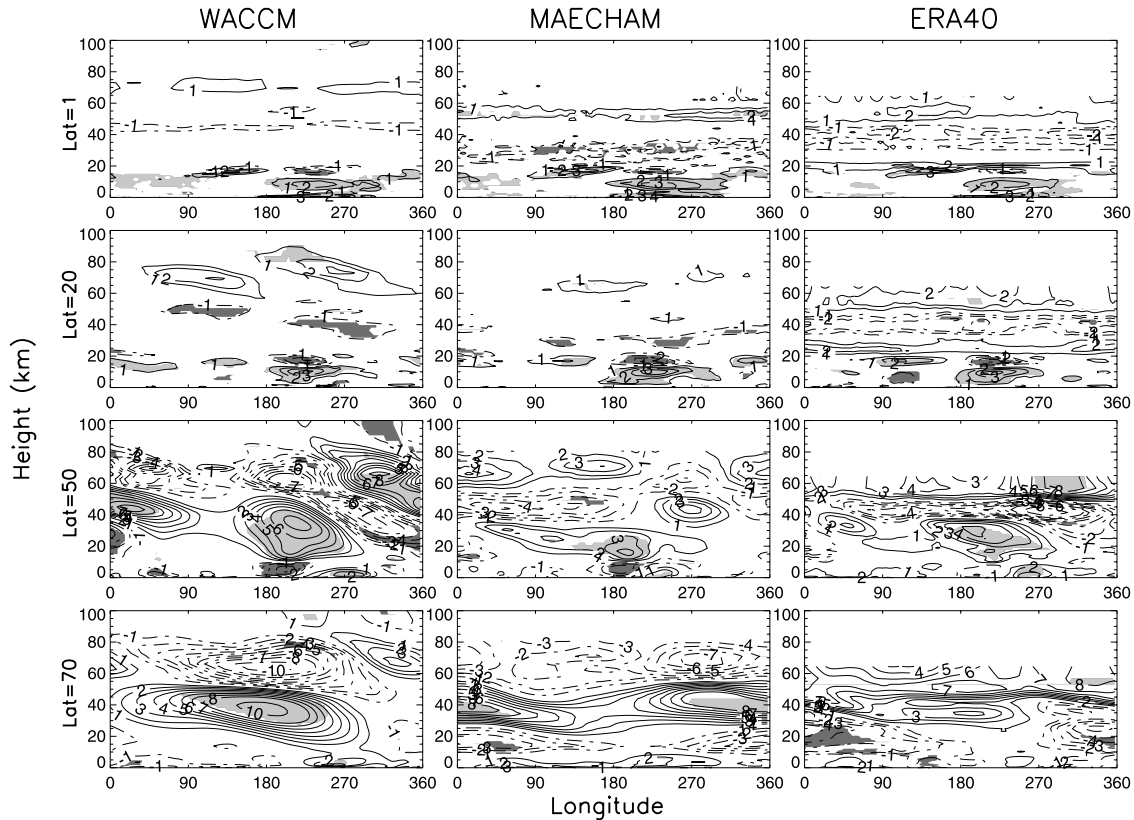


**Figure 6a.** Composite differences (warm-cold events) of temperature anomalies from (left) WACCM, (middle) MAECHAM5, and (right) ERA-40 data in month 0 at latitudes (top to bottom)  $1^{\circ}\text{N}$ ,  $20^{\circ}\text{N}$ ,  $50^{\circ}\text{N}$ , and  $70^{\circ}\text{N}$ . Solid (dashed) lines denote positive (negative) anomalies. Contour interval is  $1^{\circ}\text{C}$ . Zero contour has not been displayed. Shaded regions indicate statistically significant anomalies at the 95% confidence level. Light (dark) gray indicates positive (negative) significant anomalies.

several latitudes not previously shown (Figures 6a and 6b). This comparison between latitudes highlights the differences between hemispheres in the extratropics, and within each hemisphere. The ENSO signature changes from being confined to the first 20–25 km at tropical latitudes to propagating upward into the middle atmosphere at extratropical latitudes. The smallest significant anomalies are observed at  $30^{\circ}$ . Latitudes  $40^{\circ}$  and  $50^{\circ}$  show the most effective vertical propagation, while propagation becomes weak or less effective at higher latitudes, where the significant signal exhibits a more zonally symmetric behavior in the NH.

[22] Finally, the comparison of ENSO anomalies obtained from the three data sets provides new insights into the propagation of ENSO signals. In the extratropics, both the models and the reanalysis indicate vertical propagation of the ENSO signal via Rossby waves into the stratosphere, mainly in the NH. Apart from internal variability, ENSO is the only source of variability in WACCM and MAECHAM5 but not in ERA-40. The results show that, whatever additional sources of variability may be present in ERA-40, they do not obscure the stratospheric signal of ENSO in middle latitudes. In the tropics, the models and the reanalysis show similar anomalies below 20 km: a wave-like signal over the Eastern Pacific and positive anomalies in a more or less zonally symmetric pattern throughout the tropical region. However, above 20 km the ERA-40 data do

not show significant anomalies while WACCM and MAECHAM5 show negative anomalies with a more zonally symmetric pattern than in the extratropics. Differences between the model experiments and ERA-40 data in the tropical stratosphere are expected because the experiments do not include the QBO, which is the dominant mode of interannual variability in this region and obscures whatever ENSO signal might be present.

#### 4. Influence of the Zonal Mean Zonal Wind on the Vertical Propagation of the ENSO Signal

[23] Some of the results obtained from the analysis in the previous section highlight the differences in the vertical propagation between hemispheres, and also among the data sets. According to linear Rossby wave theory, there is a strong relationship between vertical propagation and zonal wind regimes. The Charney and Drazin (CD) criterion [Charney and Drazin, 1961; Andrews *et al.*, 1987] indicates that quasi-stationary Rossby waves can only propagate vertically where the winds are westerly and weaker than a certain “critical” value, which depends on the total horizontal wave number. Thus only ultralong Rossby waves can propagate vertically in the climatological westerly winds that prevail in the winter stratosphere. In summer, when stratospheric winds are easterly, vertical propagation of Rossby waves is not possible.

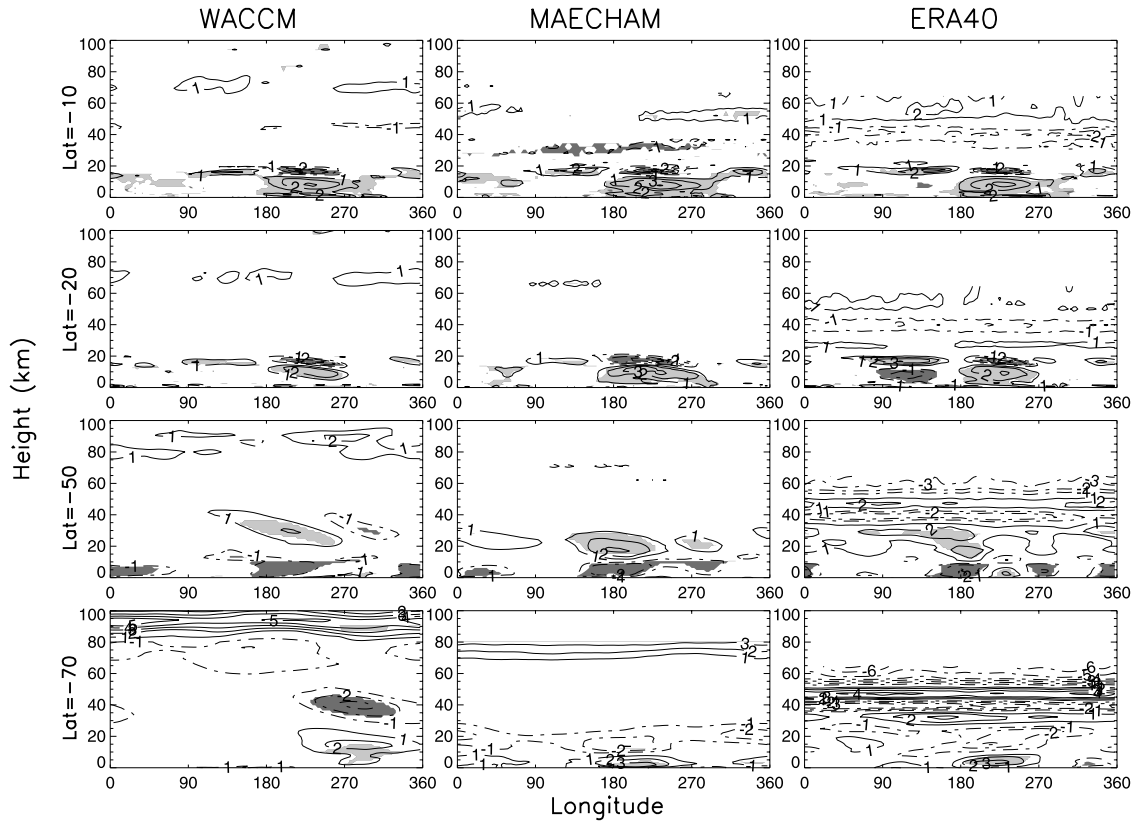


**Figure 6b.** As in Figure 6a but for latitudes (top to bottom) 10°S, 20°S, 50°S, and 70°S.

[24] Figure 7 depicts the average and standard deviation of the zonal mean zonal winds for 21 winters, from 1979 to 1999 for WACCM, MAECHAM5 and ERA-40 data. We should keep in mind that data are not reliable in the uppermost four levels in each data set as they are part of the sponge layer related to boundary conditions. That is around 0.25 hPa or 58 km in MAECHAM5 and around 0.8 hPa or 50 km in ERA-40. This constraint is not relevant in WACCM as its top is at 140 km. As expected, westerlies are observed in the NH up to the mesosphere, while in the SH easterlies are observed above 20 to 40 km. The zonal mean zonal wind distributions are almost identical in both models and the reanalysis below 20 km. Above that level, the largest differences are observed in the winter hemisphere. Reanalysis wind data reach maximum values around  $50 \text{ m s}^{-1}$  at 50 km, while maximum winds in WACCM are stronger (around  $60 \text{ m s}^{-1}$ ), and weaker in MAECHAM5 (about  $40 \text{ m s}^{-1}$ ). However, these differences are not significant because the variability associated with the wind maxima is about  $10 \text{ m s}^{-1}$ . The vertical shear is also more intense in WACCM in the NH lower stratosphere. In the SH, the models and reanalysis agree best, although at polar latitudes westerlies are observed at higher altitudes in WACCM. In the tropics, the Semi-Annual Oscillation (SAO) is present in the models, being stronger in WACCM, and it is also observed in the ERA-40 data. Variability related to the QBO is evident only in ERA-40 data, as expected.

[25] Taking into account the CD criterion discussed above, it follows that, in the Northern Hemisphere, wester-

lies help propagate the ENSO signal into the middle atmosphere. However, in the Southern Hemisphere, easterlies inhibit wave propagation above 20 km. Thus the ENSO signals are not expected to propagate vertically above about 20 km during the first few months after the month 0 of our composite differences, in agreement with our results.

[26] In the tropics, the winter climatology shows easterly zonal mean zonal winds in the whole stratosphere from 20 to 50 km. The easterly winds, together with the small group and phase velocity for the low-frequency equatorial Rossby waves present in that region [see, e.g., *Andrews et al.*, 1987], inhibit upward propagation and make the waves more susceptible to damping or even critical layer absorption. Therefore it is not surprising that the composite maps (Figure 4) show the ENSO anomalies related to Rossby wave patterns confined to the troposphere and lower stratosphere, below 20 km.

[27] The zonal mean zonal wind patterns also explain to some extent, the differences between WACCM, MAECHAM5 and ERA-40. In the Northern Hemisphere, WACCM shows more intense vertical propagation in month 0. Regarding other months, the main differences are observed 6 months after the maximum of N3.4 where MAECHAM5 shows significant anomalies up to 40 km. From month 0 onward, the westerly wind jet in the Southern Hemisphere grows and the vertical shear becomes positive in the upper SH stratosphere while the westerlies in the NH weaken (not shown). As a result, in month 6 (boreal summer), the winds pattern is almost the opposite of the pattern in month 0 (not shown). At that time, westerlies extend into



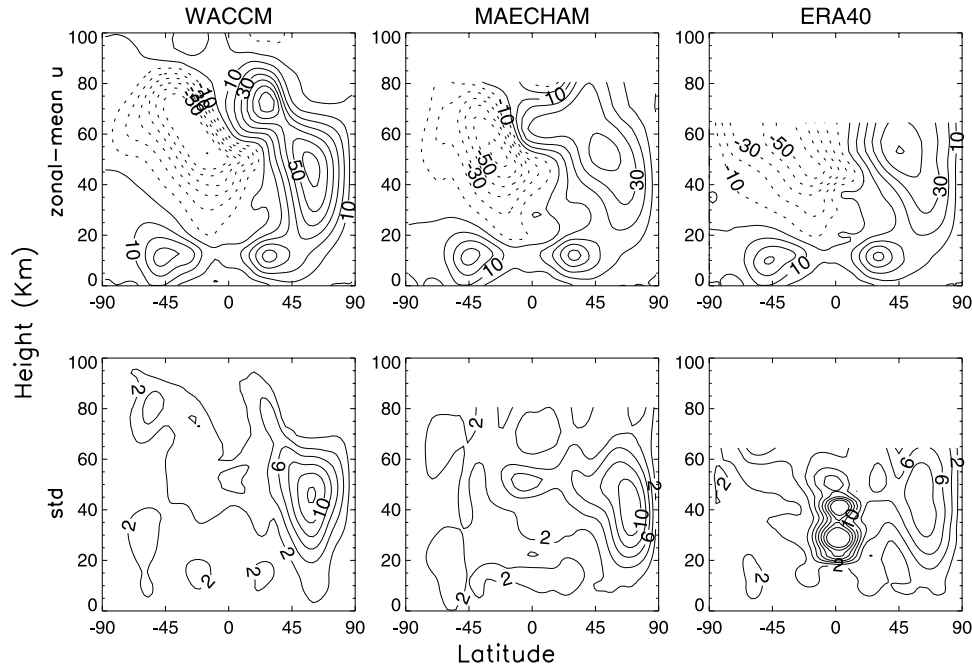


**Figure 7.** (top) Zonal mean zonal wind in boreal winter (December–January–February) and (bottom) its standard deviation for (left) WACCM, (middle) MAECHAM5, and (right) ERA-40 data. Solid (dashed) lines denote positive (negative) values. Contour interval is  $10 \text{ m s}^{-1}$  for the zonal mean zonal wind and  $2 \text{ m s}^{-1}$  for the standard deviation.

the mesosphere in the SH enhancing vertical wave propagation in that region. However, only MAECHAM5 shows vertical propagation of the ENSO signal in the Southern Hemisphere with significant ENSO-related anomalies up to 40 km. The zonal mean zonal winds in MAECHAM5 are weaker than those in ERA-40 and WACCM at those latitudes. Following CD criterion, westerlies in ERA-40 and WACCM at  $40^\circ\text{S}$  could be too strong to help vertical propagation.

### 5. Influence of the Mean Meridional Circulation on the ENSO Signal

[28] Up to this point, we have dealt with the ENSO signal transmitted upward by Rossby waves both in the tropics and extratropics. In the tropics, we have shown that a wave-like ENSO signal is present over the Pacific Ocean below 20 km. Above that altitude, ERA-40 does not show significant anomalies, but in both WACCM and MAECHAM5 a nearly zonally symmetric band of significant negative anomalies related to ENSO is observed (Figure 4). These anomalies appear mainly 3 months after the N3.4 maximum in the entire tropical area, from about  $10^\circ\text{N}$  to  $10^\circ\text{S}$  (see Figures 6a and 6b) and are observed around 20–25 km in MAECHAM5 and in the range 20–35 km in WACCM.

[29] In order to take a closer look at these zonally symmetric anomalies, Figures 8a and 8b shows composite differences of zonal mean temperature for WACCM, MAECHAM5 and ERA-40 in several months. At tropical latitudes, most of the significant anomalies in the models are located in two regions: troposphere/lower stratosphere and lower/middle stratosphere. The former, from the surface to about 15 km, shows positive anomalies during a warm

ENSO event and is evident in both models and the reanalysis, reaching their maxima between months 3 and 6 of the composites. These anomalies correspond to the well-known zonally symmetric warming that develops in the tropical troposphere during the mature phase of a warm ENSO event [e.g., Yulaeva and Wallace, 1994; Calvo et al., 2004].

[30] In the tropical stratosphere, the negative anomalies seen above 20 km in the composite differences of the total temperature field (Figure 4) are also present in the zonal mean composites of Figures 8a and 8b. These zonal mean anomalies are not significant in the reanalysis probably because of the influence of the QBO in that region, as discussed in section 3. As was the case for the anomalies presented in Figure 4, the models differ in the extent and duration of the zonal mean anomalies of Figures 8a and 8b. On the other hand, in the high latitudes of the NH, there is a dipolar structure with positive and negative anomalies centered around 40 and 70 km, respectively, in month 0 and at lower heights in the next months (around 20 and 50 km in month 3). These anomalies in the polar region of the winter hemisphere are in agreement to the model studies of Sassi et al. [2004] and Manzini et al. [2006]. In particular, the downward propagation is well analyzed for MAECHAM5 by Manzini et al. [2006]. However, in contrast to Manzini et al. [2006], who obtained warm anomalies in MAECHAM5 around half the values of those in ERA-40, our anomalies in both models and in the reanalysis are in very good agreement and reach the same amplitudes in higher latitudes (around 10 K). This is probably due to the ensemble mean used by Manzini et al. [2006], which smooth the anomalies behavior. On the other hand, the quadrupolar pattern observed by Sassi et al. [2004] for February, with anomalies in subtropical and polar

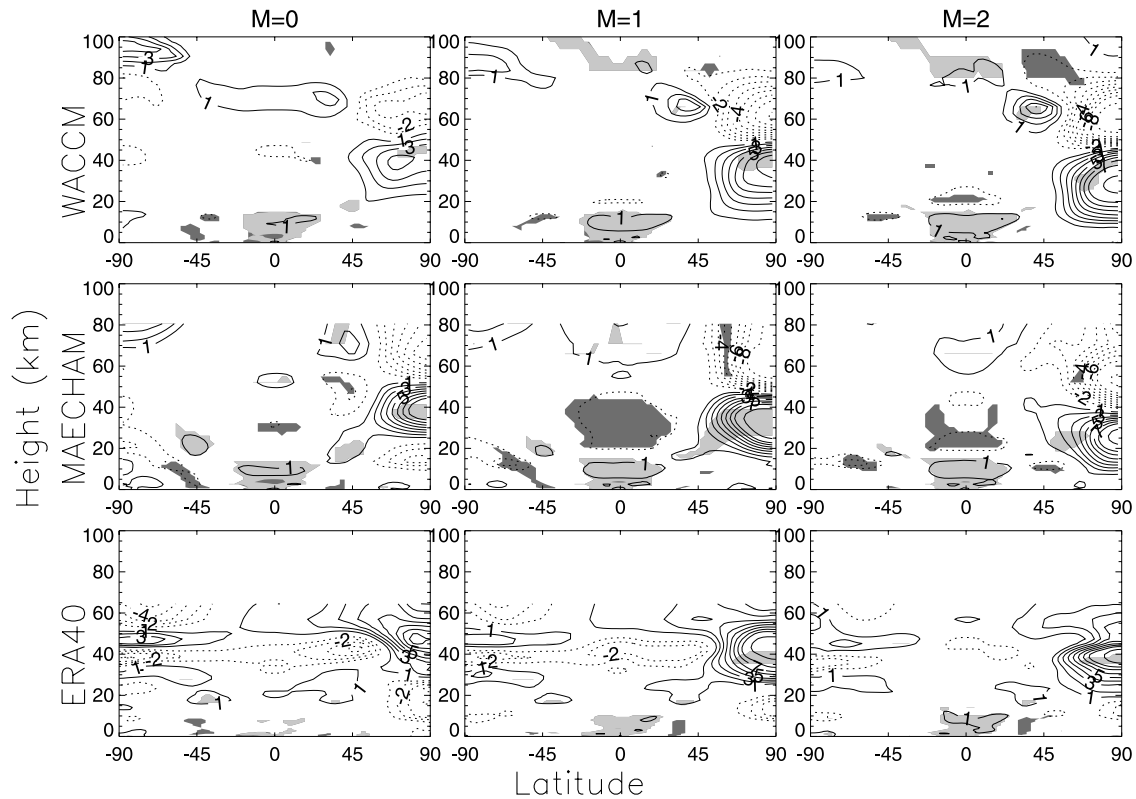


**Figure 8a.** Composite differences (warm-cold events) of zonal mean temperature anomalies from (top) WACCM, (middle) MAECHAM5, and (bottom) ERA-40 data in months (left) 0, (middle) 1, and (right) 2. Solid (dashed) lines denote positive (negative) anomalies. Shaded regions indicate statistically significant anomalies at the 95% confidence level. Light (dark) gray indicates positive (negative) significant anomalies. Contour interval is  $1^{\circ}\text{C}$ . Zero line has not been displayed.

latitudes is not observed in our analysis as our significant anomalies in tropics show a more symmetric behavior around the Equator. Finally, most of the ENSO-related anomalies in higher latitudes are related to warm ENSO events as *Sassi et al.* [2004] and *Manzini et al.* [2006] discussed although we also find some significant signal for cold events in MAECHAM5 and ERA40 (not shown).

[31] Despite the overall agreement between data sets, there are relevant differences in timing: WACCM shows significant anomalies from month 0 to month 3, with maximum values in month 3, while the duration of this pattern in MAECHAM5 is much shorter, and largest 1 month after the maximum of N3.4. ERA-40 data exhibit a smaller significant region only in months 1 and 2.

[32] All these results point to the influence of the residual circulation on middle atmosphere zonal mean temperatures during extreme ENSO events. It is well known that the mean meridional circulation is driven by planetary waves and that it controls the thermal structure of the stratosphere [Andrews et al., 1987]. Planetary waves propagate vertically into the stratosphere, where they are refracted equatorward, deposit easterly momentum and decelerate the mean flow [Edmon et al., 1980]. This deceleration is balanced by a poleward residual circulation that causes adiabatic cooling in the tropics and warming in the extratropics. Thus *Newman et al.* [2001, Plate 5] used NCEP-NCAR reanalysis data to show that a strong negative EP flux divergence

decelerates the zonal mean flow and warms the polar stratosphere. This relationship is also evident in the ERA-40 reanalysis and the models, as shown in correlations between the EP flux divergence at 30 hPa averaged from  $30^{\circ}\text{N}$  to  $75^{\circ}\text{N}$  for January and February, and the zonal mean zonal wind (Figure 9a) and temperature (Figure 9b) in March. The period used to compute the correlations has been 1979–1999. In general, the correlation coefficients are smaller in ERA-40 than in NCEP-NCAR reanalysis. Regarding the models, WACCM correlation coefficients are higher than those in MAECHAM5 (maxima of 0.60 versus 0.45), suggesting a stronger link between EP flux divergence and zonal mean winds and temperatures. In addition, the region of influence of EP flux divergence on the zonal wind varies depending on the data sets; it extends into the upper stratosphere in WACCM (similar to NCEP-NCAR reanalysis used by *Newman et al.* [2001]), while it is concentrated in the lower stratosphere in MAECHAM5 more similar to ERA-40 reanalysis. The agreement for the temperature/EP flux divergence correlation patterns is better, which shows a strong influence of the EP flux divergence of January–February on polar temperature (from  $60^{\circ}$  northward) during March in the lower stratosphere. However, the correlation coefficients in ERA-40 are much smaller than those in NCEP-NCAR or in the reanalysis, maybe related to data errors in the North Pole.

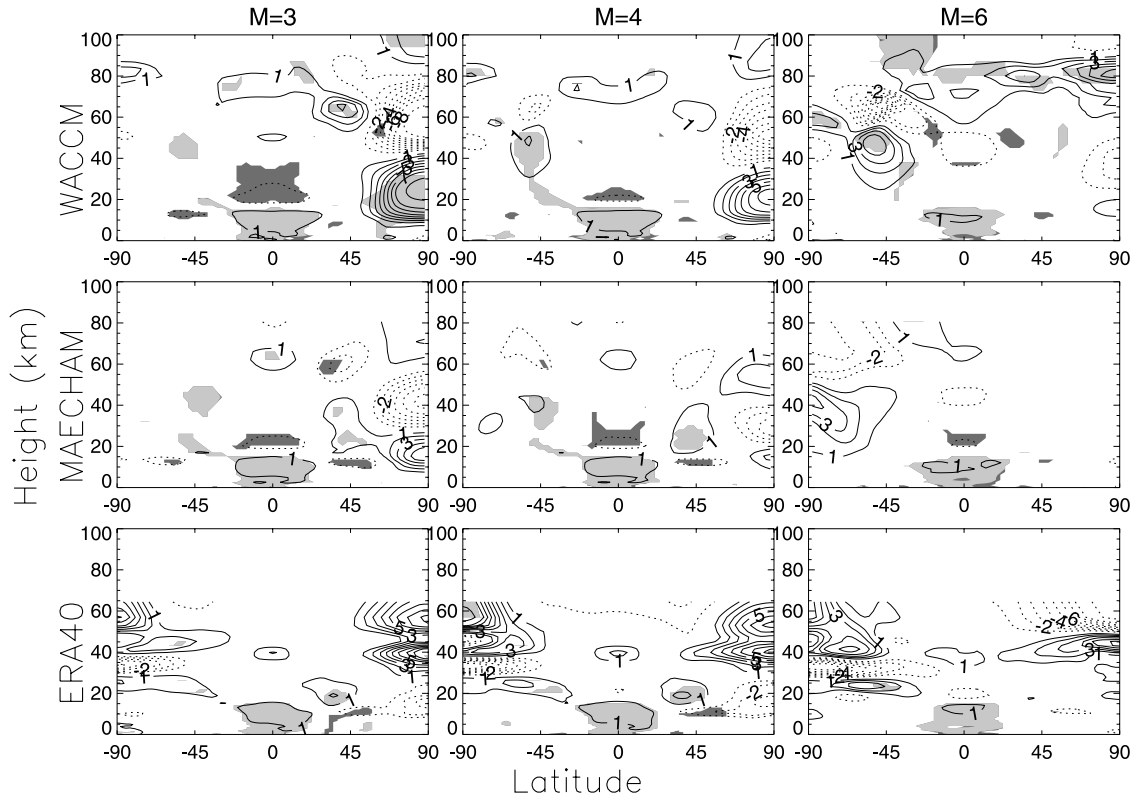


**Figure 8b.** As in Figure 8a but for months (left) 3, (middle) 4, and (right) 6.

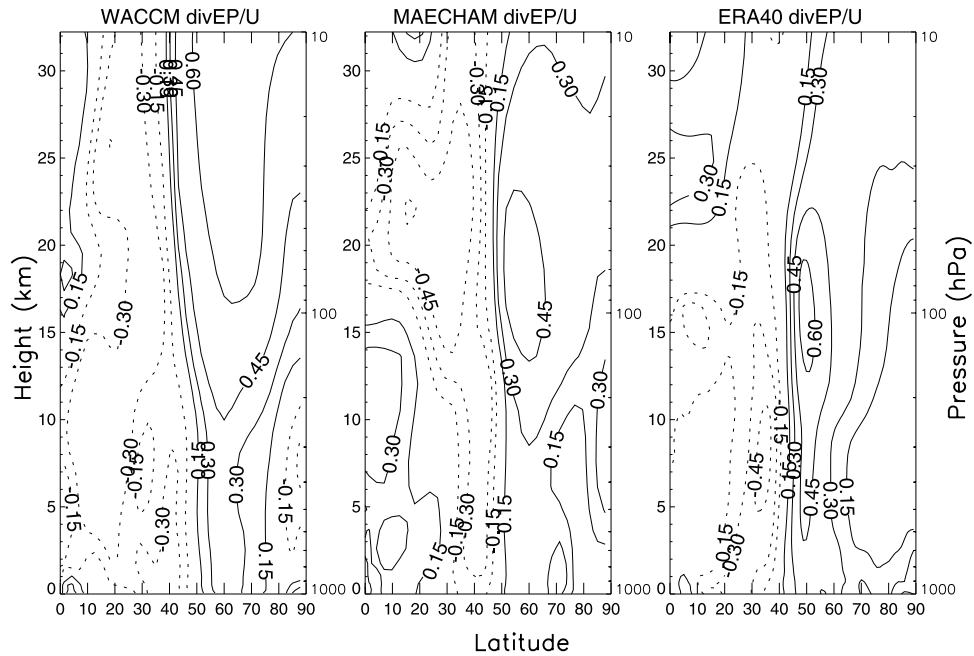


**Figure 9a.** Correlation coefficients between EP flux divergence at 30 hPa between 30°N and 75°N averaged for January–February and zonal mean zonal wind anomalies in March from (left) WACCM, (middle) MAECHAM5, and (right) ERA-40 data. Solid (dashed) lines denote positive (negative) correlation coefficients. Contour interval is 0.15.

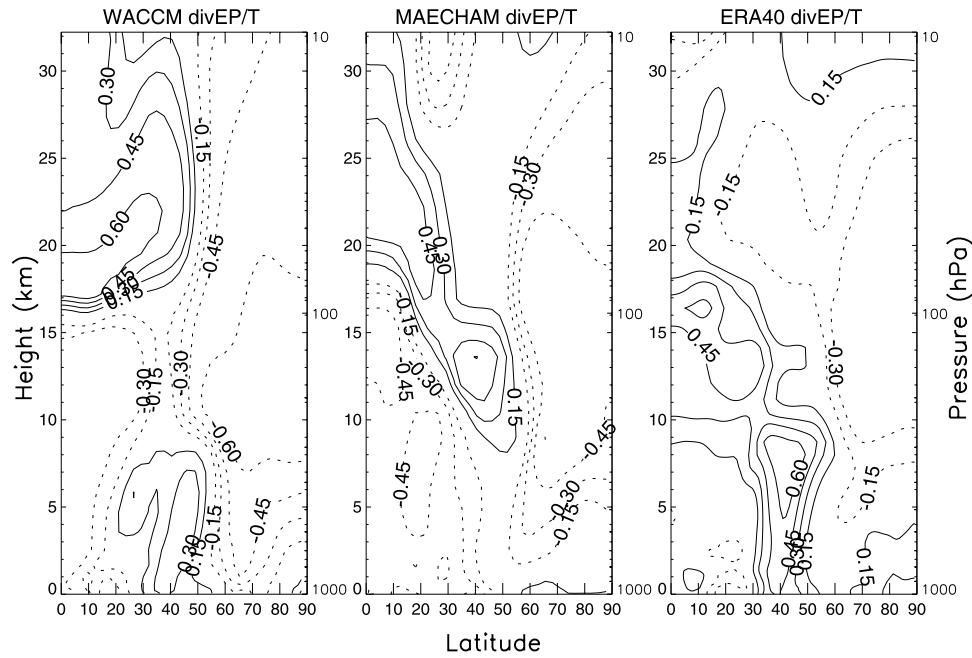


**Figure 9b.** As in Figure 9a but for the correlation coefficients between EP flux divergence at 30 hPa between 30°N and 75°N averaged for January–February and zonal mean temperature anomalies in March.

[33] Having established the relationship between wave driving, meridional circulation and zonal temperatures, we analyze how this is modified during extreme ENSO events. To that end, Figure 10 shows composite differences of the anomalies of the residual circulation (arrows) and anomalies of the EP flux divergence (contours) for WACCM and MAECHAM5 at months 0 and 3. During a warm ENSO event, the stratospheric branch of the Brewer-Dobson (BD) circulation is enhanced in the winter hemisphere. This is due to the anomalous vertical propagation and dissipation of Rossby waves during ENSO events. In a warm event the convergence of EP flux increases at high levels and enhances the BD circulation (cf. Figures 5 and 10). These anomalies in the residual circulation produce the zonal mean temperature anomalies seen in Figures 8a and 8b in the polar regions. However, anomalies in the zonal mean temperature reach their largest significant values at different times: in month 1 in MAECHAM5, between months 1 and 2 in ERA-40, and in month 3 in WACCM. This is in agreement with the anomalies in vertical propagation of planetary waves in WACCM (Figure 5), as the waves are refracted equatorward earlier in MAECHAM5 than in WACCM (month 0 versus 3 respectively); and also with the duration of the positive anomalies in the residual circulation, which enhance the BD circulation during a longer time in WACCM than in MAECHAM. Negative circulation anomalies are observed for the first time in month 3 in MAECHAM5, but between months 4 and 5 in WACCM (not shown).

[34] Summing up, during a warm ENSO event, an enhancement of planetary wave vertical propagation and the residual circulation occurs. This produces cooling in the tropics and warming in the polar regions in the winter hemisphere. However, in the real atmosphere only the polar

warming is observed because the ENSO-related anomalies are probably overshadowed by signals related to other sources of variability, such as the QBO in the tropical stratosphere.

## 6. Conclusions

[35] In this paper, we have analyzed the ENSO signal on atmospheric temperatures using reanalysis data (ERA-40) and two general circulation models, WACCM and MAECHAM5. The global coverage and vertical resolution of the models and the reanalysis make them suitable candidates for investigating the propagation of the ENSO signal into the middle atmosphere. Further, comparing results in the middle atmosphere from all these sources also provides a good opportunity to improve the understanding of the physical mechanisms involved.

[36] Focusing first on the overall agreement obtained among ERA-40, WACCM and MAECHAM5, our main conclusions are twofold:

[37] 1. Our analysis shows that the ENSO signal propagates toward the middle atmosphere by means of ultralong Rossby waves. This vertical propagation depends strongly on latitude. It is mainly observed in the extratropics, with maxima at 40°–50° and is weaker and less effective at higher latitudes. It has been shown that the zonal mean zonal wind regimes exert a strong influence on the propagation of the ENSO signal. This propagation is more effective at middle latitudes in the Northern Hemisphere, where ENSO wave-like anomalies are observed up to 35–40 km. This is due mainly to the timing of the ENSO maxima with respect to the seasonal cycle, (usually boreal winter, so westerly winds are present throughout the NH stratosphere in month 0 while easterlies in the SH inhibit



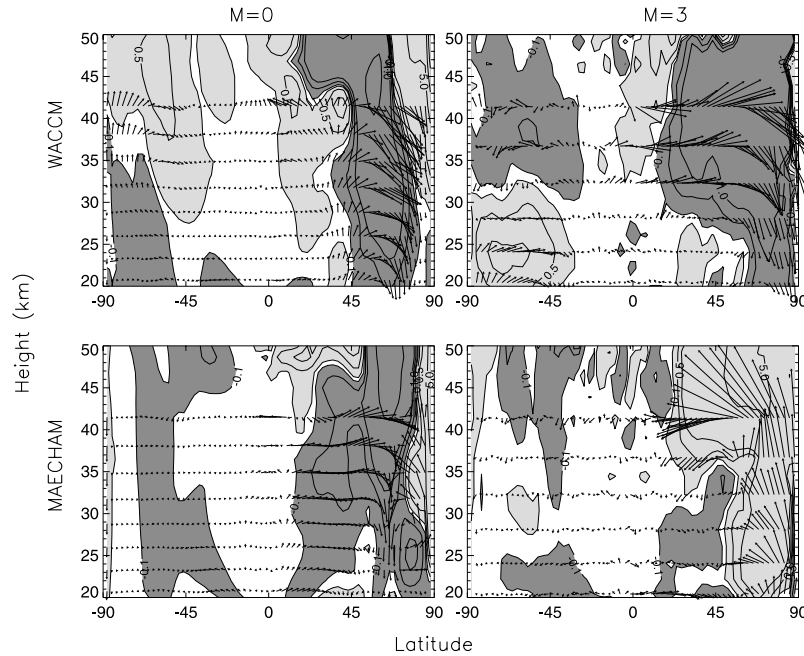


**Figure 10.** Composite differences (warm-cold events) of the anomalies of the residual circulation (arrows) and divergence of the EP flux (contours) computed from (top) WACCM and (bottom) MAECHAM5 data in months (left) 0 and (right) 3. EP flux divergence is given in  $\text{m s}^{-1} \text{d}^{-1}$ . Contours are drawn at 0.1, 0.5, 1, 5, and then every 5  $\text{m s}^{-1} \text{d}^{-1}$ , the same for negative divergence. Regions are shadowed for positive or negative divergence larger than 0.1.

vertical propagation in accordance to CD criterion), and also to differences in the zonal mean zonal wind regimes between hemispheres. In the tropics, the small group and phase velocity of the equatorially Rossby waves, together with the easterly zonal mean zonal winds present there, confine vertical propagation of the ENSO signal by Rossby waves to the troposphere and lowermost stratosphere.

[38] 2. We have also shown that ENSO wave-like anomalies are not the only ones observed in the middle atmosphere. The analysis of the zonal mean temperature, residual circulation and EP flux divergence during large ENSO events shows that ENSO also generates anomalies in zonal mean temperature in the stratosphere in polar regions. During the warm phase of ENSO, the anomalous vertical propagation of Rossby waves into the stratosphere forces an enhancement of the winter stratospheric branch of the BD circulation, which in turn causes cooling in the tropics and warming in high latitudes. This is in agreement with *Chen et al.* [2003], who suggested that SSTs could affect the winter stratospheric circulation and also with the model studies of *Sassi et al.* [2004] and *Manzini et al.* [2006].

[39] The comparison of the results between models highlights some interesting differences. WACCM shows greater anomalies of vertical wave propagation into the middle atmosphere and the largest differences between Northern and Southern Hemisphere propagation. Examination of the zonal mean zonal wind climatologies of the two models reveals that WACCM winds are generally more intense than those in ERA-40, while the winds in MAECHAM5 are less intense than those in the reanalysis. The relationship among EP flux divergence, the residual circulation, and the zonal mean zonal winds and temperatures in high latitudes is well

established in both models, being stronger in WACCM. Finally, the residual circulation anomalies are less intense in MAECHAM5, and show shorter duration. This is also related to differences in the timing of the zonal mean temperature anomalies observed in the polar winter region: maximum anomalies are observed earlier in MAECHAM5 than in WACCM: mainly 1 month after the maximum of N3.4 in MAECHAM5, in months 1 and 2 in ERA-40 and 3 months after the maximum of N3.4 in WACCM.

[40] The influence of other sources of variability on the propagation of the ENSO signal may be estimated by considering that ERA-40 includes all of them whereas, apart from internal variability, the only such source present in the models is ENSO. Thus, below 20 km, the models and the ERA-40 data are in very good agreement, indicating that ENSO dominates other sources of variability in the troposphere and lower stratosphere [cf. *Calvo et al.*, 2004]. Above the lower stratosphere, the reasonably good agreement among the models and the reanalysis in middle latitudes indicates that middle latitudes do not seem to be influenced significantly by other external phenomena. However, in the tropical stratosphere ERA-40 does not show any significant ENSO-related anomalies in zonal mean temperature, whereas the models do. This discrepancy is probably due to the influence of the QBO in the tropical stratosphere, which obscures any ENSO signal that might be present.

[41] **Acknowledgments.** This paper has been partially funded by NCAR and MPI, which, additionally, kindly provided the data from the models. Furthermore, we want to thank the National Institute of Meteorology (INM) in Spain and the ECMWF for facilitating the access to the ERA-40 data.

## References

- Andrews, D. G., J. R. Holton, and C. B. Leovy (1987), *Middle Atmospheric Dynamics, Int. Geophys. Ser.*, vol. 40, 489 pp., Elsevier, New York.
- Angell, J. K. (1981), Comparison of variations in atmospheric quantities with sea surface temperature variations in the equatorial eastern Pacific, *Mon. Weather Rev.*, **109**, 230–243.
- Angell, J. K. (2000), Tropospheric temperature variations adjusted for El Niño, 1958–1998, *J. Geophys. Res.*, **105**, 11,841–11,849.
- Baldwin, M. P., and D. O'Sullivan (1995), Stratospheric effects of ENSO-related tropospheric circulation anomalies, *J. Clim.*, **8**, 649–667.
- Calvo, N., R. García, R. García Herrera, D. Gallego, L. Gimeno, E. Hernández, and P. Ribera (2004), Analysis of the ENSO signal in tropospheric and stratospheric temperatures observed by MSU, 1979–2000, *J. Clim.*, **17**, 3934–3946.
- Charney, J. G., and P. G. Drazin (1961), Propagation of planetary-scale disturbances from the lower into the upper atmosphere, *J. Geophys. Res.*, **66**, 83–109.
- Chen, W., M. Takahashi, and H.-F. Graf (2003), Interannual variations of stationary planetary wave activity in the northern winter troposphere and stratosphere and their relations to NAM and SST, *J. Geophys. Res.*, **108**(D24), 4797, doi:10.1029/2003JD003834.
- Christy, J. R., and R. T. McNider (1994), Satellite greenhouse signal, *Nature*, **367**, 325.
- Díaz, H. F., M. P. Hoerling, and J. K. Eischeid (2001), ENSO variability, teleconnections and climate change, *Int. J. Clim.*, **21**, 1845–1862.
- Edmon, H. J., Jr., B. J. Hoskins, and M. E. McIntyre (1980), Eliassen-Palm cross sections for the troposphere, *J. Atmos. Sci.*, **37**, 2600–2616.
- García, R., and M. L. Salby (1987), Transient response to localized episodic heating in the tropics. Part II: Far-field behavior, *J. Atmos. Sci.*, **44**, 499–530.
- Giorgetta, M. A., E. Manzini, and E. Roeckner (2002), Forcing of the quasi-biennial oscillation from a broad spectrum of atmospheric waves, *Geophys. Res. Lett.*, **29**(8), 1245, doi:10.1029/2002GL014756.
- Halpert, M. S., and C. S. Ropelewski (1992), Surface temperature patterns associated with the Southern Oscillation, *J. Clim.*, **5**, 577–593.
- Hamilton, K. (1993), An examination of observed Southern Oscillation effects in the Northern Hemisphere stratosphere, *J. Atmos. Sci.*, **50**, 3468–3473.
- Horel, J. D., and J. M. Wallace (1981), Planetary-scale atmospheric phenomena associated with the Southern Oscillation, *Mon. Weather Rev.*, **109**, 813–829.
- Horinouchi, T., and S. Yoden (1996), Excitation of transient waves by localized episodic heating in the tropics and their propagation into the middle atmosphere, *J. Meteorol. Soc. Jpn.*, **74**, 189–210.
- Hoskins, B. J., and D. Karoly (1981), The steady linear response of a spherical atmosphere to thermal and orographic forcing, *J. Atmos. Sci.*, **38**, 1179–1196.
- Kiehl, J. R., J. J. Hack, G. B. Bonan, B. A. Bobille, D. L. Williamson, and P. J. Rasch (1998), The National Center for Atmospheric Research Community Climate Model, CCM3, *J. Clim.*, **11**, 1131–1149.
- Kiladis, G. N., and H. F. Diaz (1989), Global climatic anomalies associated with extremes in the Southern Oscillation, *J. Clim.*, **2**, 1069–1090.
- Manzini, E., N. A. McFarlane, and C. McLandress (1997), Impact of the Doppler spread parameterization on the simulation of the middle atmosphere circulation using the MA/ECHAM4 general circulation model, *J. Geophys. Res.*, **102**, 25,751–25,762.
- Manzini, E., M. A. Giorgetta, M. Esch, L. Kornbluth, and E. Roeckner (2006), The influence of sea surface temperatures on the northern winter stratosphere: Ensemble simulations with the MAECHAM5 model, *J. Clim.*, in press.
- Newman, P. A., E. R. Nash, and J. E. Rosenfield (2001), What controls the temperature of the Arctic stratosphere during the spring?, *J. Geophys. Res.*, **106**, 19,999–20,010.
- Oort, A. H., and J. J. Yienger (1996), Observed interannual variability in the Hadley circulation and its connection to ENSO, *J. Clim.*, **9**, 2751–2767.
- Randel, W., et al. (2004), The SPARC intercomparison of middle-atmosphere climatologies, *J. Clim.*, **17**, 986–1003.
- Reid, G. C., K. S. Gage, and J. R. McAfee (1989), The thermal response of the tropical atmosphere to variations in equatorial Pacific sea surface temperature, *J. Geophys. Res.*, **94**, 14,705–14,716.
- Ribera, P., and M. E. Mann (2002), Interannual variability in the NCEP reanalysis 1948–1999, *Geophys. Res. Lett.*, **29**(10), 1494, doi:10.1029/2001GL013905.
- Roeckner, E., K. Arpe, L. Bengtsson, M. Christoph, M. Claussen, L. Dümenil, M. Esch, M. Giorgetta, U. Schlese, and U. Schulzweida (1996), The atmospheric general circulation model ECHAM-4: Model description and simulation of present day climate, *MPI-Rep. 219*, Max Planck Inst. for Meteorol., Hamburg, Germany.
- Roeckner, E., et al. (2003), The atmospheric general circulation model ECHAM 5. Part I: Model description, *Rep. 349*, Max Planck Inst. for Meteorol., Hamburg, Germany. (Available at <http://www.mpimet.mpg.de>.)
- Sassi, F., R. R. Garcia, B. A. Boville, and H. Liu (2002), On temperature inversions and the mesospheric surf zone, *J. Geophys. Res.*, **107**(D19), 4380, doi:10.1029/2001JD001525.
- Sassi, F., D. Kinnison, B. A. Boville, R. R. Garcia, and R. Roble (2004), Effect of El Niño–Southern Oscillation on the dynamical, thermal, and chemical structure of the middle atmosphere, *J. Geophys. Res.*, **109**, D17108, doi:10.1029/2003JD004434.
- Simmons, A. J., and J. K. Gibson (2000), The ERA-40 project plan, *ERA-40 Proj. Rep. Ser. 1*, 63 pp., Eur. Cent. for Medium-Range Weather Forecasts, Reading, U. K.
- Simmons, A. J., J. M. Wallace, and W. Branstator (1983), Barotropic wave propagation and instability, and atmospheric teleconnection patterns, *J. Atmos. Sci.*, **40**, 1363–1392.
- Uppala, S., P. Kallberg, A. Hernandez, S. Saarinen, M. Fiorino, X. Li, K. Onogi, N. Sokka, U. Andrae, and V. Da Costa Bechtold (2004), ERA-40: ECMWF 45-year reanalysis of the global atmosphere and surface conditions 1957–2002, *ECMWF Newsl.*, **101**, 2–21.
- van Loon, H., and K. Labitzke (1987), The Southern Oscillation. Part V: The anomalies in the lower stratosphere of the Northern Hemisphere in winter and a comparison with the quasi-biennial oscillation, *Mon. Weather Rev.*, **109**, 149–155.
- Wallace, J. M., and F.-C. Chang (1982), Interannual variability of the wintertime polar vortex in the Northern Hemisphere middle stratosphere, *J. Meteorol. Soc. Jpn.*, **60**, 149–155.
- Wallace, J. M., and D. S. Gutzler (1981), Teleconnections in the geopotential height field during the Northern Hemisphere winter, *Mon. Weather Rev.*, **109**, 784–812.
- Williamson, D. L. (1997), Climate simulations with a spectral, semi-Lagrangian model with linear grids, in *Numerical Methods in Atmospheric and Ocean Modelling*, edited by C. Lin, R. Laprise, and H. Ritchie, pp. 279–292, Can. Meteorol. and Oceanogr. Soc., Ottawa.
- Williamson, D. L., and J. G. Olson (1994), Climate simulations with a semi-Lagrangian version of the NCAR Community Climate Model, *Mon. Weather Rev.*, **122**, 1594–1610.
- Yulaeva, E., and J. M. Wallace (1994), The signature of ENSO in global temperature and precipitation fields derived from the microwave sounding unit, *J. Clim.*, **7**, 1719–1736.

N. Calvo and R. García-Herrera, Dpto. de Física de la Tierra II, Universidad Complutense de Madrid, Avda. Complutense s/n E-28040 Madrid, Spain. (nataliac@fis.ucm.es)

R. R. García, National Center for Atmospheric Research, Boulder, CO 80307-3000, USA.

M. A. Giorgetta, Max Planck Institute for Meteorology, D-20146 Hamburg, Germany.